Nonlinear Analysis: Modelling and Control, 2007, Vol. 12, No. 1, 113–122

Effect of Variable Thermal Conductivity on Buoyant Convection in a Cavity with Internal Heat Generation

S. Sivasankaran

UGC-DRS Center for Fluid Dynamics
Department of Mathematics, Bharathiar University
Coimbatore-641046, Tamil Nadu, India
sdsiva@gmail.com

Received: 11.08.2006 **Revised:** 08.10.2006 **Published online:** 29.01.2007

Abstract. A numerical study has been made to analyze the effects of variable thermal conductivity on the natural convection of heat generating fluids contained in a square cavity with isothermal walls and the top and bottom perfectly insulated surfaces. The flow is assumed to be two-dimensional. Calculations are carried out by solving governing equations for different parameters. The flow pattern and the heat transfer characteristics inside the cavity are presented in the form of steady-state streamlines, isotherms and velocity profiles. The heat transfer rate is increased by an increase in the thermal conductivity parameter.

Keywords: buoyant convection, internal heat generation, variable thermal conductivity.

1 Introduction

Convective heat transfer in an enclosure is important in many engineering applications including heat exchangers, nuclear reactors and cooling of electronic systems. Acharya and Goldstein [1] numerically investigated the natural convection in a cavity containing uniformly distributed internal energy sources. Hossain and Rees [2] studied natural convection flow of water subject to density inversion in a rectangular cavity with internal heat generation. It is found that the circulation of the flow is reversed when heat generation parameter is sufficiently strong. Joshi *et al.* [3] analytically studied the natural convection in a cavity with volumetric heat generation. They found that a lower order solution is adequate to capture the natural convection in the cavity. Natural convection in an inclined enclosure with internal heat generation is studied by Kandaswamy and Sivasankaran [4]. They found that the rate of heat transfer is increased when the source strength is increased.

Kim and Hyun [5] examined buoyancy induced convection with internal heat generation under time periodic thermal boundary condition. Transient natural convection with variable fluid properties in an enclosure by integral transform technique is investigated by Leal *et al.* [6]. Saravanan and Kandaswamy [8] studied the effect of variable thermal

conductivity on natural convection driven by the combined mechanism of buoyancy and surface tension in the presence of a uniform vertical magnetic field. They found that the heat transfer across the cavity from hot wall to cold wall becomes poor for a decrease in the thermal conductivity in the presence of magnetic field.

Sun and Emery [9] examined the conjugate natural convection of air filled enclosure containing internal heat sources and an internal baffle. They found that the average heat flux ratio along hot wall increases monotonically in the absence of an internal energy source. Sundaravadivelu and Kandaswamy [10] investigated the convection of water in the vicinity of its density maximum temperature (277 K) in an inclined square cavity in the presence of heat sources. They found that the multiple fluid vortices exist inside the cavity due to temperature of maximum density and the size of these vortices is find to vary strongly on the inclination angle and the heat source parameter. The present study addresses the effect of variable thermal conductivity of a heat generating fluid contained in a square cavity.

2 Mathematical formulation

The physical system under consideration is a two dimensional square cavity of size L as shown in Fig. 1. The vertical side walls of the cavity are isothermal but maintained at different temperatures θ_h (hot wall) and θ_c (cold wall) with $\theta_h > \theta_c$. The horizontal walls are thermally insulated. The thermal conductivity of the liquid k is assumed to vary linearly with temperature as $k = k_c - a(\theta - \theta_c)$, where a is the temperature coefficient of thermal conductivity and the subscript c refers to the reference state at the cold wall. u and v are the velocity components in x and y directions respectively.

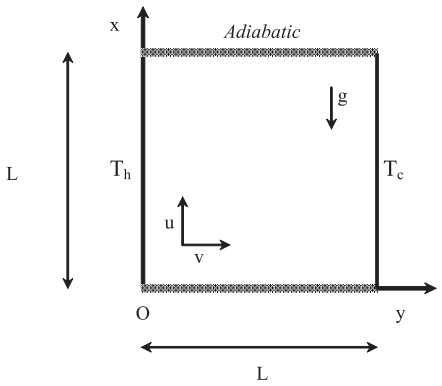

Fig. 1. Physical configuration.

The equations governing the motion of the laminar two-dimensional incompressible flow of the heat generating fluid under consideration are,

$$\frac{\partial u}{\partial x} + \frac{\partial v}{\partial y} = 0, \tag{1}$$

$$\frac{\partial u}{\partial t}+u\frac{\partial u}{\partial x}+v\frac{\partial u}{\partial y}=-\frac{1}{\rho_0}\frac{\partial p}{\partial x}+\nu\nabla^2 u-g\beta(\theta-\theta_c), \tag{2}$$

$$\frac{\partial v}{\partial t}+u\frac{\partial v}{\partial x}+v\frac{\partial v}{\partial y}=-\frac{1}{\rho_0}\frac{\partial p}{\partial y}+\nu\nabla^2 v, \tag{3}$$

$$\frac{\partial \theta}{\partial t}+u\frac{\partial \theta}{\partial x}+v\frac{\partial \theta}{\partial y}=\alpha\Bigg\{\left[1-\frac{a(\theta-\theta_c)}{k_c}\right]\nabla^2\theta - \frac{a}{k_c}\left[\left(\frac{\partial\theta}{\partial x}\right)^2+\left(\frac{\partial\theta}{\partial y}\right)^2\right]\Bigg\}+\frac{Q}{\rho_0 c_p}, \tag{4}$$

where g is the gravitational force, p is the pressure, t is the time, Q is the rate of heat generation, c_p is the specific heat, α is the thermal diffusivity, β is the coefficient of thermal expansion, ρ_0 is the density of the fluid at θ_c, θ is the temperature and ν is the kinametic viscosity.

The appropriate initial and boundary conditions are:

$$\begin{aligned}
t=0\colon\quad & u=v=0, \quad \theta=\theta_c; \quad 0\le x,y\le L,\\
t>0\colon\quad & u=v=0, \quad \frac{\partial\theta}{\partial x}=0; \quad x=0,\ x=L,\\
& u=v=0, \quad \theta=\theta_h; \quad y=0,\\
& u=v=0, \quad \theta=\theta_c; \quad y=L.
\end{aligned}$$

In order to obtain a finite-volume analogue we transform the above equations by means of the following transformation:

$$X=\frac{x}{L},\quad Y=\frac{y}{L},\quad U=\frac{u}{\nu/L},\quad V=\frac{v}{\nu/L},\quad \tau=\frac{t}{L^2/\nu},\quad \Psi=\frac{\psi}{\nu},$$
$$\zeta=\frac{\omega}{\nu/L^2},\quad T=\frac{\theta-\theta_c}{\theta_h-\theta_c},\quad Q=\frac{S\nu\rho_0 c_p(\theta_h-\theta_c)}{L^2},$$

where T is the non-dimensional temperature, ζ is the non-dimensional vorticity, ω is the dimensional vorticity, Ψ is the non-dimensional stream function, ψ is the dimensional stream function, S is the heat generation parameter and τ is the non-dimensional time.

The vorticity-stream function formulation of the problem (1)–(4) after nondimensionalization can be written as,

$$\frac{\partial\zeta}{\partial\tau}-\frac{\partial\Psi}{\partial Y}\frac{\partial\zeta}{\partial X}+\frac{\partial\Psi}{\partial X}\frac{\partial\zeta}{\partial Y}=\nabla^2\zeta+Gr\frac{\partial T}{\partial Y}, \tag{5}$$

$$\nabla^2\Psi=-\zeta, \tag{6}$$

$$\frac{\partial T}{\partial \tau} - \frac{\partial \Psi}{\partial Y}\frac{\partial T}{\partial X} + \frac{\partial \Psi}{\partial X}\frac{\partial T}{\partial X} = \frac{1}{Pr}\Bigg\{\nabla^2 T - \eta\Bigg[T\frac{\partial^2 T}{\partial X^2} + T\frac{\partial^2 T}{\partial Y^2} \left(\frac{\partial T}{\partial X}\right)^2 + \left(\frac{\partial T}{\partial Y}\right)^2\Bigg]\Bigg\} + S, \quad (7)$$

$$U = -\frac{\partial \Psi}{\partial Y}, \quad V = \frac{\partial \Psi}{\partial X} \quad \text{and} \quad \zeta = \frac{\partial U}{\partial Y} - \frac{\partial V}{\partial X}. \quad (8)$$

The initial and boundary conditions in the dimensionless form are

$$\begin{aligned}
&\tau = 0; \quad \Psi = 0; && T = 0; \quad 0 \le X \le 1; \quad 0 \le Y \le 1,\\
&\tau > 0; \quad \Psi = \frac{\partial \Psi}{\partial Y} = 0; && \frac{\partial T}{\partial X} = 0; \quad X = 0 \,\&\, 1; \quad 0 \le Y \le 1,\\
&\qquad\quad \Psi = \frac{\partial \Psi}{\partial X} = 0; && T = 1; \quad Y = 0; \qquad 0 \le X \le 1,\\
&\qquad\quad \Psi = \frac{\partial \Psi}{\partial X} = 0; && T = 0; \quad Y = 1; \qquad 0 \le X \le 1.
\end{aligned}$$

The non-dimensional parameters that appear in the equations are $Gr = \frac{g\beta(\theta_h - \theta_c)L^3}{\nu^2}$, the Grashof numbers, $Pr = \frac{\nu}{\alpha}$, the Prandtl number and $\eta = \frac{a(\theta_h - \theta_c)}{k_c}$, the thermal conductivity parameter. The local Nusselt number is defined by $Nu = \frac{\partial T}{\partial Y}\Big|_{Y=0}$, resulting in the average Nusslet number as $\overline{Nu} = \int_0^1 Nu\, dX$.

3 The method of solution

The governing equations (5)–(8) were discretized using the finite volume formulation, with power law scheme, Patankar [7]. At each time step the vorticity and temperature distributions were obtained from equations (5) and (7) respectively. The resulting set of discretized equations for each variable were solved by Gauss Seidal method. The stream function distribution was obtained from equation (6) by using Successive Over Relaxation method. The dimensionless time step which yielded convergence was taken to be $\tau = 10^{-4}$. We fixed the relaxation parameter to be 1.5. The velocity components are then found using central difference approximations. After finding all the values at a particular level, the values at the higher levels were similarly computed. This computational cycle was repeated for each of the next levels and steady state solution was obtained when the convergent criteria $|\Phi_{i,j,n} - \Phi_{i,j,n+1}| < 10^{-5}$ for temperature, vorticity and stream function had been met. The overall Nusselt number was also used to develop an understanding of what grid fineness is necessary for accurate numerical simulations. The numerical solution were done for different grid system from 21×21 to 101×101. After 41×41 grids, there is no considerable change in average Nusselt number. So 41×41 grid is used to find solutions for different parameters.

4 Results and discussions

The effect of thermal conductivity variation on natural convection induced by internal heat generation is investigated numerically. The computations have been done for the various values of the heat source parameter S, the thermal conductivity parameter η, that is, $S = 1, 10$ and 25, $\eta = 0, 0.001, 0.005, 0.01$ and 0.05 and the Grashof numbers from 10^3 to 10^6. The isotherms for $S = 25$ and various values of η are displayed in Figs. 2(a)–(e). When $\eta = 0.001$, the isotherms are more attracted to the cold wall. It is clearly seen from the Fig. 2(b), that the temperature inside the cavity is slightly increased than the boundary temperature due to internal heat generation. The isotherms are attracted towards the hot wall and form the thermal boundary layer for the case $\eta = 0.05$. When $\eta = 0.05$, the isotherms are almost parallel straight lines near the vertical walls. But, for low values of η, no sharp boundary layer can be seen. We notice that the isotherms near the hot wall begin to crowd and start forming a thermal boundary layer as η increases. The corresponding streamlines are depicted in the Figs. 3(a)–(e). When a square cavity containing a mass of incompressible fluid is heated through the hot wall, the fluid starts moving along the hot wall. This motion induces a circulation of the fluid within the cavity and reaches the steady state over time. When $\eta = 0$ and $S = 25$, there exists a bicellular flow pattern with

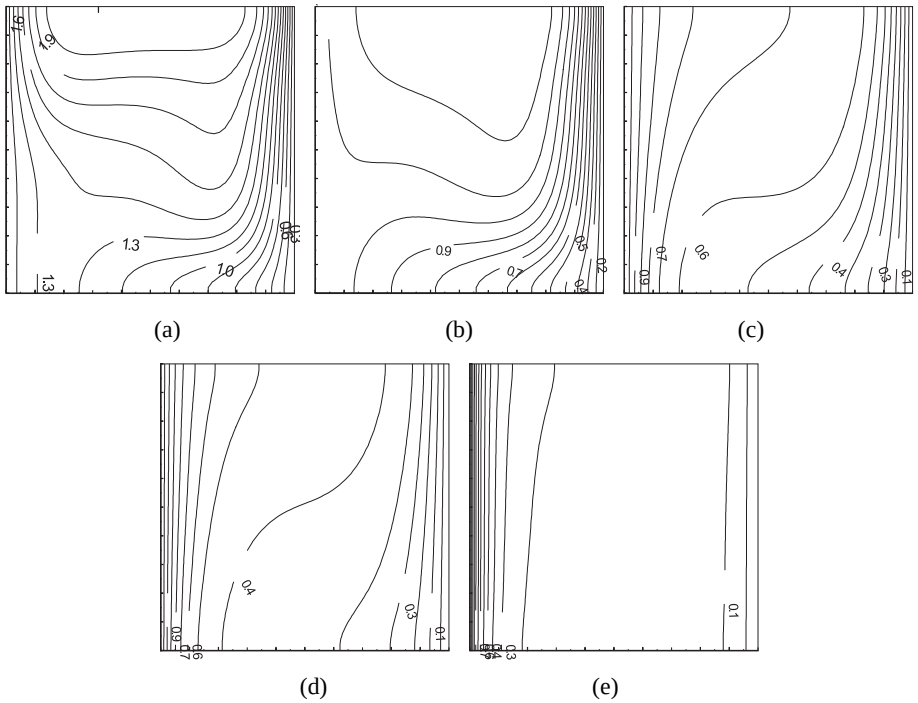

Fig. 2. Isotherms for $S = 25$, $Gr = 20000$, $Pr = 0.732$ and different η: (a) $\eta = 0$; (b) $\eta = 0.001$; (c) $\eta = 0.005$; (d) $\eta = 0.01$; (e) $\eta = 0.05$.

a large vortex near the cold wall and a small vortex near the top corner of the hot wall, Fig. 3. As η is increased further, the vortex along the hot wall, Fig. 3(b), is suppressed in its size and finally a single vortex arises. Then a unicellular flow behaviuor results and occupies the entire cavity.

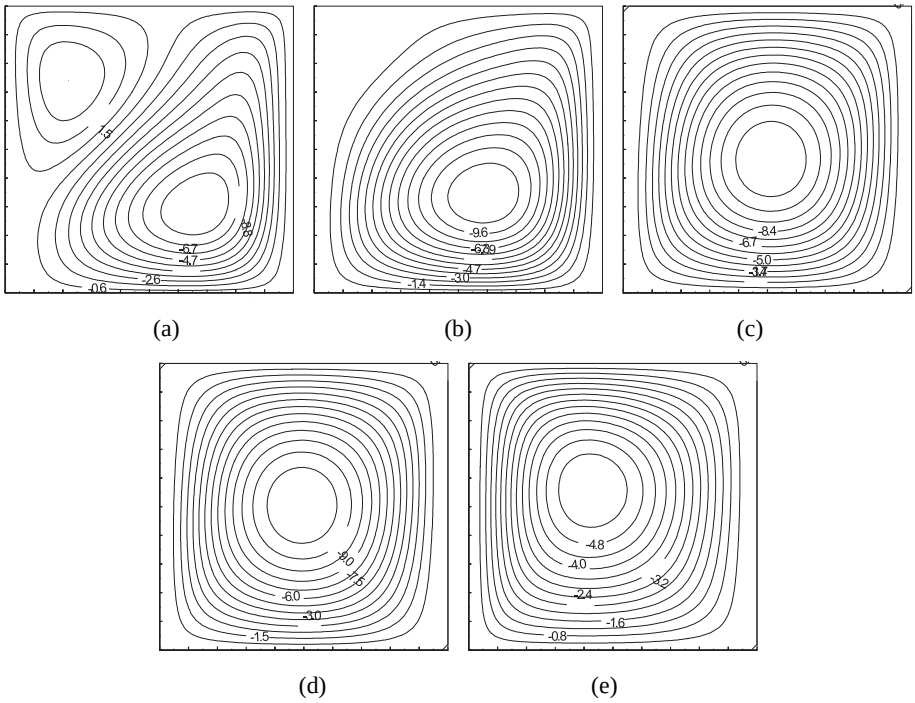

(a) (b) (c)

(d) (e)

Fig. 3. Streamlines for $S = 25$, $Gr = 20000$, $Pr = 0.732$ and different η: (a) $|\Psi_{max}| = 9.8$ $\eta = 0$; (b) $|\Psi_{max}| = 10.4$, $\eta = 0.001$; (c) $|\Psi_{max}| = 10.9$, $\eta = 0.005$; (d) $|\Psi_{max}| = 9.8$, $\eta = 0.01$; (e) $|\Psi_{max}| = 5.2$, $\eta = 0.05$.

Figs. 4(a)–(c) show the isotherms for $\eta = 0, Gr = 20000, Pr = 0.732$ and increasing S. Increasing the source parameter S increases the internal energy of the fluid. The corresponding streamlines are depicted in the Figs. 5(a)–(c). The eddy in Fig. 5(a) circulates in the counterclockwise direction and occupies the whole cavity, that is, the movement of the eddy is downward along the hot wall and upward along the cold wall. There exists a small clockwise rotating cell near the hot wall top corner for increasing S. On further increasing S the hot cell grows in its size and strengthens. Figs. 6(a)–(d) show the isotherms for different Grashof numbers. When $Gr = 10^3$, the isotherms indicate that convection mode of heat transfer is started. On further increasing the Grashof numbers convection is dominated. The isotherms are attracted towards both hot and cold walls for higher values of Grashof number. Figs. 7(a)–(d) show the flow pattern for different Grashof numbers. There exists a unicellular flow pattern occupying the whole cavity for

all values of Grashof numbers. The circulation rate of the eddy is increased by increasing the Grashof number. This is clearly seen from the $|\Psi|_{max}$ values indicated in the Figures.

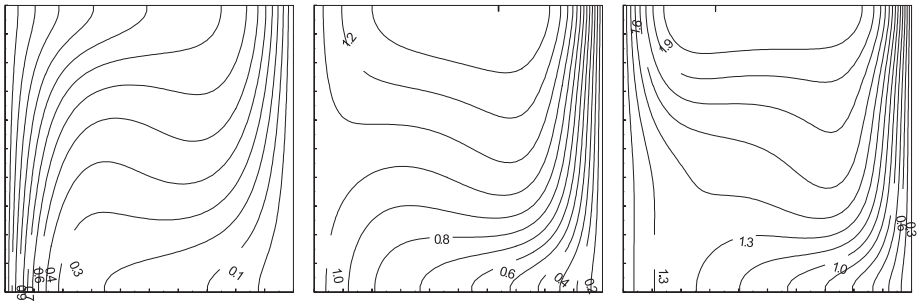

(a) (b) (c)

Fig. 4. Isotherms for $\eta = 0,\ Gr = 20000,\ Pr = 0.732$ and different S: (a) $S = 1$; (b) $S = 10$; (c) $S = 25$.

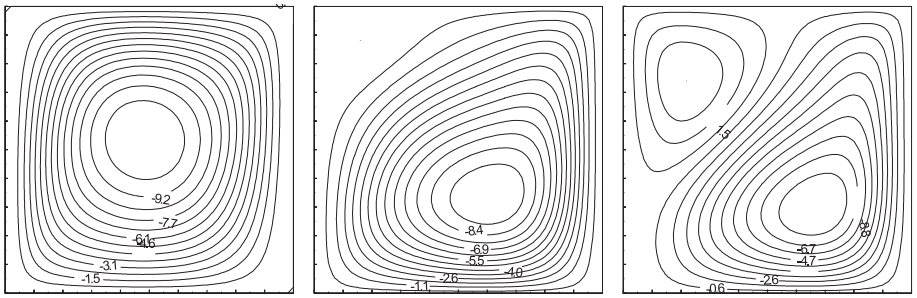

(a) (b) (c)

Fig. 5. Streamlines for $\eta = 0, Gr = 20000, Pr = 0.732$ and different S: (a) $\Psi_{max} = 10$, $S = 1$; (b) $\Psi_{max} = 9.3$, $S = 10$; (c) $\Psi_{max} = 9.8$, $S = 25$.

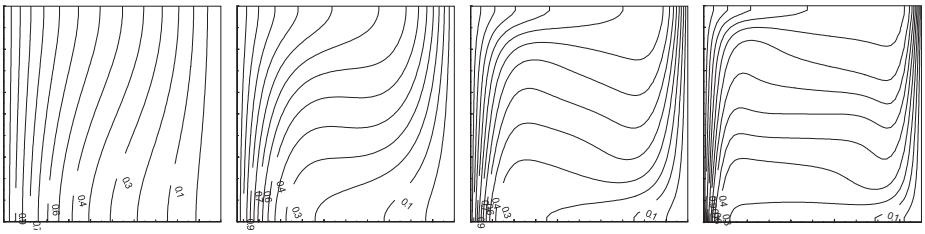

(a) (b) (c) (d)

Fig. 6. Isotherms for $\eta = 0.001, S = 1.0, Pr = 0.732$ and different Grashof numbers: (a) $Gr = 10^3$; (b) $Gr = 10^4$; (c) $Gr = 10^5$; (d) $Gr = 10^6$.

The rate of heat transfer is calculated in terms of the average heat transfer coefficient $\overline{Nu}$ at the hot wall of the cavity. The $\overline{Nu}$ serves as a measure for the heat transfer rate. The time history of $\overline{Nu}$ for different values of η are displayed in Fig. 8. As time evolves the particles near the hot wall have higher temperature and so the heat transfer rate starts decreasing thus resulting in a sudden fall in the graph. Finally the steady state is reached and the $\overline{Nu}$ is seen to become constant. It is found to increase with the increase in the variable thermal conductivity parameter η. Average Nusselt number for various values of η and S are depicted in Figs. 9 and 10. Heat transfer rate increases when the variable thermal conductivity parameter is increased. It is found that the heat transfer rate is reduced in the presence of heat sources. Fig. 11 shows the average Nusselt number for different Grashof numbers. It is found that the heat transfer rate is increased with increase in the Grashof number. The velocity profiles for $S = 1$ and $Gr = 2 \times 10^4$ are depicted in the Fig. 12. Fig. 13 shows the mid-height velocity profiles for different Grashof numbers. The velocity of the fluid particles inside the cavity is increased for increased Grashof numbers.

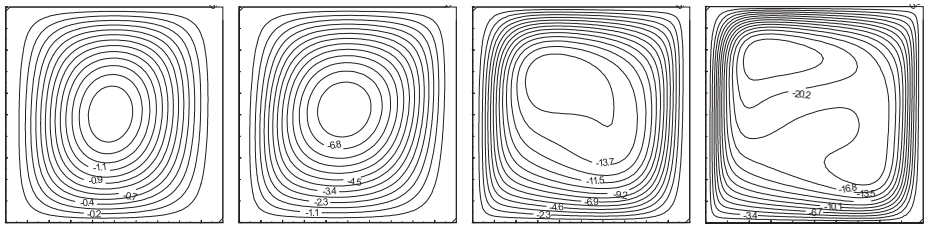

(a) (b) (c) (d)

Fig. 7. Streamlines for $\eta = 0.001$, $S = 1.0$, $Pr = 0.732$ and different Grashof numbers: (a) $\Psi_{max} = 1.4$, $Gr = 10^3$; (b) $\Psi_{max} = 7.4$, $Gr = 10^4$; (c) $\Psi_{max} = 14.9$, $Gr = 10^5$; (d) $\Psi_{max} = 21.9$, $Gr = 10^6$.

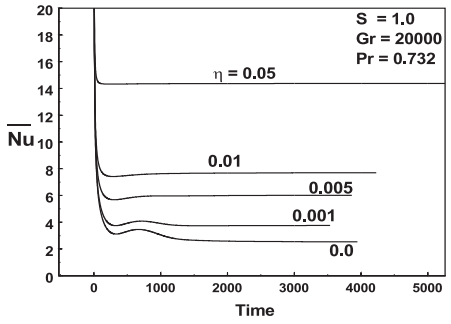

Fig. 8. Time history of Average Nusselt number for various η.

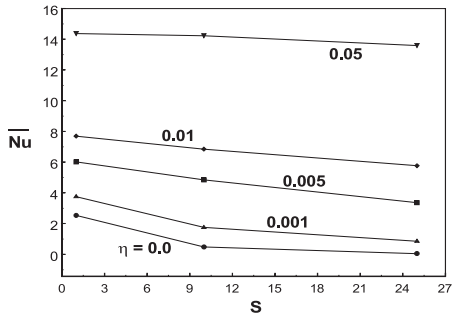

Fig. 9. Average Nusselt number for various η.

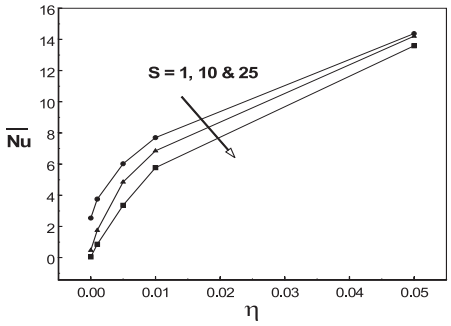

Fig. 10. Average Nusselt number for various S.

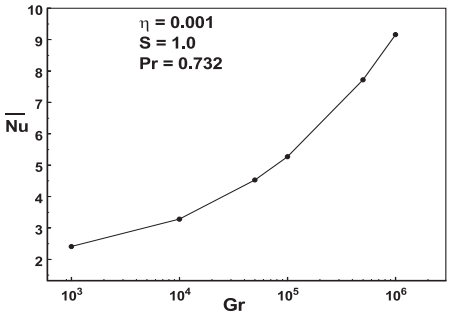

Fig. 11. Average Nusselt number Vs Grashof numbers.

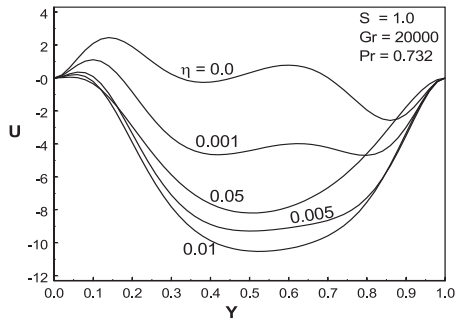

Fig. 12. Mid-height velocity profiles for various η.

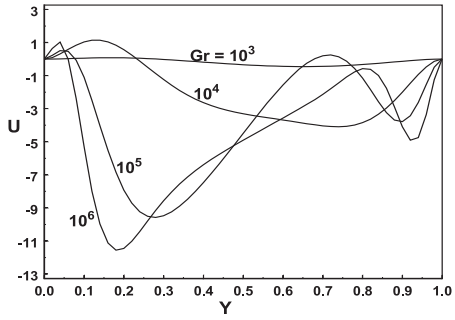

Fig. 13. Mid-height velocity profile for different Grashof numbers.

5 Conclusions

The natural convection of heat generating fluids contained in a square cavity with variable thermal conductivity is studied numerically. The heat transfer is mainly due to convection and the rate of heat transfer increases with the increase in the thermal conductivity parameter. Heat transfer rate is reduced in the presence of heat sources.

References

1. S. Acharya, R. J. Goldstein, Natural convection in an externally heated vertical or inclined square box containing internal energy sources, *J. Heat Transfer*, **107**(4), pp. 855–865, 1985.
2. M. A. Hossain, D. A. S. Rees, Natural convection flow of water near its density maximum in a rectangular enclosure having isothermal walls with heat generation, *Heat Mass Transfer*, **41**(4), pp. 367–374, 2005.

3. M. V. Joshi, U. N. Gaitonde, S. K. Mitra, Analytical study of natural convection in an cavity with volumetric heat generation, *J. Heat Transfer*, **128**(2), pp. 176–182, 2006.

4. P. Kandaswamy, S. Sivasankaran, Natural Convection in an inclined enclosure with internal heat generation, *Proc. Nat. Acad. Sci., India, A*, **76**(2), pp. 145–150, 2006.

5. G. B. Kim, J. M. Hyun, Enclosed Buoyant Convection with internal heat generation under oscillating sidewall temperature, *J. Heat Transfer*, **124**(3), pp. 577–580, 2002.

6. M. A. Leal, H. A. Machado, R. M. Cotta, Integral transform solutions of transient natural Convection in enclosures with variable fluid properties, *Int. J. Heat Mass Transfer*, **43**(21), pp. 3977–3990, 2000.

7. S. V. Patankar, *Numerical heat transfer and fluid flow, Hemisphere*, McGraw-Hill, Washington, DC, 1980.

8. S. Saravanan, P. Kandaswamy, Low Prandtl number magnetoconvection in cavities: Effect of variable thermal conductivity, *ZAMM*, **80**(8), pp. 570–576, 2000.

9. Y. S. Sun, A. F. Emery, Effects of wall conduction, internal heat sources and an internal baffle on natural convection heat transfer in an rectangular enclosure, *Int. J. Heat Mass Transfer*, **40**(4), pp. 915–929, 1997.

10. K. Sundaravadivelu, P. Kandaswamy, Natural convection of water in inclined cavity with heat generation, *J. Appl. Math. Computing*, **12**(1–2), pp. 281–289, 2003.